Human Ferrochelatase: Characterization of Substrate−Iron Binding and Proton-Abstracting Residues†

Vera M. Sellers,‡ Chia-Kuei Wu,§ Tamara A. Dailey,§ and Harry A. Dailey*,‡,§

Department of Microbiology, Department of Biochemistry and Molecular Biology, and Center for Metalloenzyme Studies, University of Georgia, Athens, Georgia 30602-7229

Received January 3, 2001; Revised Manuscript Received May 24, 2001

ABSTRACT: The terminal step in heme biosynthesis, the insertion of ferrous iron into protoporphyrin IX to form protoheme, is catalyzed by the enzyme ferrochelatase (EC 4.99.1.1). A number of highly conserved residues identified from the crystal structure of human ferrochelatase as being in the active site were examined by site-directed mutagenesis. The mutants Y123F, Y165F, Y191H, and R164L each had an increased K_m for iron without an altered K_m for porphyrin. The double mutant R164L/Y165F had a 6-fold increased K_m for iron and a 10-fold decreased V_{max}. The double mutant Y123F/Y191F had low activity with an elevated K_m for iron, and Y123F/Y165F had no measurable activity. The mutants H263A/C/N, D340N, E343Q, E343H, and E343K had no measurable enzyme activity, while E343D, E347Q, and H341C had decreased V_{max}s without significant alteration of the K_ms for either substrate. D340E had near-normal kinetic parameters, while D383A and H231A had increased K_ms for iron. On the basis of these data and the crystal structure of human ferrochelatase, it is proposed that residues E343, H341, and D340 form a conduit from H263 in the active site to the protein exterior and function in proton extraction from the porphyrin macrocycle. The role of H263 as the porphyrin proton-accepting residue is central to catalysis since metalation only occurs in conjunction with proton abstraction. It is suggested that iron is transported from the exterior of the enzyme at D383/H231 via residues W227 and Y191 to the site of metalation at residues R164 and Y165 which are on the opposite side of the active site pocket from H263. This model should be general for mitochondrial membrane-associated eucaryotic ferrochelatases but may differ for bacterial ferrochelatases since the spatial orientation of the enzyme within prokaryotic cells may differ.

Ferrochelatase (protoheme ferrolyase, EC 4.99.1.1) catalyzes the terminal step in heme biosynthesis, the insertion of ferrous iron into protoporphyrin IX to form protoheme IX (heme) (*1*, *2*). In eukaryotes, the enzyme is nuclear-encoded, synthesized in the cytoplasm, and translocated to the mitochondrion where it is proteolytically processed to its mature size of ∼42 kDa (*3*). Within the mitochondria, ferrochelatase is associated with the inner mitochondrial membrane with the active site facing the mitochondrial matrix (*4*, *5*). Ferrochelatase has been isolated from a variety of sources, and the gene encoding the enzyme has been cloned and sequenced from more than 40 species, including bacteria (*6*−*9*), yeast (*10*), plants (*11*), and animals (*12*−*15*). Overall, there are fewer than 10% of the residues in the core portion of the enzyme that are identical in all known ferrochelatases. An NO-sensitive [2Fe-2S] cluster has been identified and characterized in recombinant animal ferrochelatases (*15*−*21*), but it is absent in the plant enzymes.

Available data on substrate specificity and kinetic parameters indicate that the mechanism of catalysis is conserved, although substrate specificity varies slightly among species (see ref *1* and references therein). Mammalian ferrochelatase utilizes Fe^{2+} as the physiological metal substrate; however, other divalent cations such as Co^{2+} and Zn^{2+} can serve as alternate substrates. *Bacillus subtilis* ferrochelatase is unusual in the utilization of Cu^{2+}, and not Co^{2+}, as an acceptable substrate in vitro (*22*). In all ferrochelatases, Hg^{2+}, Mn^{2+}, and Cd^{2+} are strong inhibitors while Pb^{2+} is a less effective inhibitor (*1*, *22*, *23*). Ferrochelatase is thought to utilize an ordered reaction mechanism where iron binds prior to porphyrin (*24*). Following the binding of the metal ion, distortion of the porphyrin to a nonplanar conformation facilitates porphyrin metalation (*25*−*27*). This distortion has been demonstrated by resonance Raman spectroscopy to be a doming (*26*, *28*) or ruffling (*29*) of the porphyrin macrocycle. Concomitant with metalation of the macrocycle, two protons are removed from pyrrole nitrogens.

Details of the enzyme mechanism along with the nature of the specific amino acids involved in catalysis remain largely unknown. Recently, the three-dimensional structure of *B. subtilis* ferrochelatase (*30*) along with the structure of the enzyme−*N*-methylmesoporphyrin complex were published (*27*). These data clearly demonstrated the orientation of the distorted macrocycle in the active site with the center of the porphyrin ring centered directly over the equivalent

† This work was supported by grants from the National Institutes of Health (DK32303 and DK35989 to H.A.D.) and by the National Science Foundation Training Group Award to the Center for Metalloenzyme Studies (BIR9413236).

* To whom correspondence should be addressed: Department of Biochemistry and Molecular Biology, University of Georgia, Athens, GA 30602-7229. Telephone: (706) 542-2690. Fax: (706) 542-7567. E-mail: hdailey@arches.uga.edu.

‡ Department of Microbiology.

§ Department of Biochemistry and Molecular Biology and Center for Metalloenzyme Studies.

10.1021/bi010012c CCC: $20.00
Published on Web 07/25/2001

of human H263, and provide strong support for the macrocycle distortion model for iron insertion. In this investigation, a combination of site-directed mutagenesis and kinetic analyses in conjunction with the recently determined structure of human ferrochelatase (*31*) is used to study selected active site residues in human ferrochelatase. A model for metalation and porphyrin deprotonation is proposed on the basis of these data that is consistent with solution-based metalation models, but varies from models previously proposed by others for ferrochelatase. In addition, it is proposed that iron is initially bound on a surface of the enzyme that is distinct and physically separated from the active site pocket. Iron is then shuttled to the site of metalation via a series of highly conserved residues.

MATERIALS AND METHODS

Bacterial Strains and Enzyme Purification. All recombinant human ferrochelatase plasmids were expressed in *Escherichia coli* strain JM109 (*17*). In some experiments, proteins were expressed in *E. coli* Δ*hem H*, which lacks any endogenous ferrochelatase activity, to determine if the expressed protein had any in vivo activity that could complement these cells (*6*, *8*). Recombinant wild-type and mutant His-tagged human ferrochelatases were expressed and purified as previously described (*32*).

Construction of Mutants. All mutants constructed in the current work were verified by sequencing the expression cDNA. For H263 mutants, the entire coding region of the expression vector was sequenced twice from both directions to confirm that no additional mutations were present. The mutants D340E, E343D, D383A, H230A, H231A, H263A, and H263C were produced using the previously described method of Deng and Nikoloff (*33*). The plasmid pHDTF20, containing wild-type human ferrochelatase, was used as a template (*17*). The procedure was modified by performing the extension reactions at higher temperatures to improve primer specificity using high-temperature Vent DNA Polymerase and Taq DNA Ligase (New England Biolabs, Boston, MA) at the T_m of the mutagenic primer. Positive clones were confirmed by double-stranded sequencing by the *f*mol sequencing procedure (Promega, Madison, WI).

D383A, D340N, E343Q, E347Q, H230A, W227Y, R164L/C, Y165F, R164L/Y165F, Y191C/A/H, and Y123F were generated following the Quikchange protocol of Stratagene (La Jolla, CA). Both sense and antisense primers containing the required alterations were produced for each mutation. Colonies were screened by sequencing of purified double-stranded plasmid DNA by the *f*mol sequencing procedure (Promega) or by the Molecular Genetics Instrumentation Facility at the University of Georgia.

Determinations. Protein concentrations were determined spectrophotometrically using an extinction coefficient of 46 900 M^{-1} cm^{-1} at 278 nm. The intactness of the [2Fe-2S] cluster was accessed by the presence of characteristic spectra, and when possible, the stoichiometry was determined using the 330 nm peak ($\epsilon_M = 6000$ M^{-1} cm^{-1}). Enzyme activity was measured with ferrous iron and protoporphyrin IX (Porphyrin Products, Logan, UT) as substrates using a modification of a real-time direct spectroscopic assay (*2*). Assay mixtures contained 100 mM Tris-HCl (pH 8.1), 0.5% Tween 20, 10−100 μM protoporphyrin IX, and 10−120 μM ferrous ammonium sulfate. Approximately 1 nmol of ferrochelatase was added last to start the reaction, and assays were conducted at 25 °C. Activity is expressed as the number of nanomoles of heme per minute per nanomole of ferrochelatase. Kinetic parameters were determined from data sets of 10−14, assays and the reported values represent averages of three experiments with less than 10% deviation.

Determination of the Amount of Protein-Bound Porphyrin. For quantitation of protoporphyrin associated with the E343K mutant, a sample of the purified protein was placed into 2.7 N HCl and centrifuged to remove the denatured protein, and the resulting supernatant was analyzed by UV−visible absorption spectroscopy. Peaks at 410, 556, and 600 nm were observed, and the respective extinction coefficients of 262, 13.5, and 5.57 mM^{-1} cm^{-1} were utilized to determine the amount of protoporphyrin in the sample (*34*).

RESULTS

Characteristics of Carboxylate Mutants. The conserved residues D340, E343, and E347 (Figure 1 and Table 1) which were altered via site-directed mutagenesis had enzyme activity significantly different from that of the wild-type human enzyme (Table 2). All of these purified mutant enzymes have intact [2Fe-2S] clusters and are as stable upon storage as the wild-type recombinant human ferrochelatase. In mutants D340E, E343D, and E347Q, the K_ms for iron and porphyrin substrates are similar to those of the wild-type enzyme but the V_{max}s for both E343D and E347Q are decreased approximately 8-fold compared to that of the wild-type ferrochelatase. For mutants D340N, E343K, E343H, and E343Q, measurable enzyme activity is absent. Interestingly, all of these inactive mutants are purified with a significant amount of protoporphyrin bound to the protein (Figure 2), and it was found that the nature of the amino acid substitution at E343 has an effect upon the amount of bound protoporphyrin, with the greatest amounts being present in the E343K mutant enzyme. The porphyrin content of E343K was analyzed and found to be that of protoporphyrin IX with a stoichiometry of 0.4−0.5 porphyrin molecule/ferrochelatase monomer. Upon storage at 4 °C for several days, none of the bound protoporphyrin (absorbance maximum at 410−413 nm) was converted into protoheme (absorbance maximum at 424 nm). This is in contrast to wild-type ferrochelatase which as purified via the His-tag procedure occasionally has an absorbance indicative of a mixture of both bound protoporphyrin and protoheme which is all converted to protoheme within minutes of isolation (unpublished observations).

Characteristics of Aromatic Mutants. Y123 and Y165 were mutated to phenylalanine since this replacement preserves the size and aromatic nature yet removes the polar hydroxyl functional group of these residues. Both of these ferrochelatases have intact [2Fe-2S] clusters, and as shown in Table 2, Y123F has a 2-fold increased K_m for iron and a slightly lowered V_{max} while Y165F has a 50% increased K_m for iron and an increased V_{max}. The double mutant Y123F/Y165F has only minimal enzyme activity which was too low to obtain accurate kinetic data. Y191H was produced since it is a known human erythropoietic protoporphyria missense mutation (*35*). This mutant enzyme exhibits a 4-fold increased K_m for iron, but little change in the V_{max} or K_m for porphyrin.

Table 1: Conserved Amino Acid Residues of Ferrochelatase[a]

identical residues		highly conserved residues			
G77	Q302	V85	P168	V287	E347
P79	S303	F88	M177	W301	I348
D95[b]	W310	L89	P192	G306	L381
R115[b]	L311	L107[b]	S195	L311	V385
Y123	P313	I111[b]	W227	D316	
S130	F337	I132	I241	P334	
P131	E343	G127	S261	D340	
H263		G128	L265	I342	
P266		R164	G273	T344	
Y276		Y165	D274	L345	

[a] The numbering is for human ferrochelatase. This analysis is based upon 44 eukaryotic and prokaryotic ferrochelatase sequences in public databases. Identical residues are those that occur in more than 95% of the sequences. Highly conserved residues are those with conservative replacements in more than 95% of the sequences. [b] These residues are identical or highly conserved in ferrochelatases that possess this protein segment.

Table 2: Effect of Amino Acid Replacements on the Activity of Human Ferrochelatase

altered residue	K_m^{Fe} (μM)	K_m^{proto} (μM)	V_{max} (min^{-1})
none (R115L)	9.3	9.0	6.6
D340E	9.1	11.2	5.7
D340N	−	−	0
E343D	9.8	12.3	0.7
E343Q/H/K[a]	−	−	0
E347Q	9.8	12.3	0.8
H341C	8.3	ND[b]	1.9
H263A/C/N/M[a]	−	−	0
W227Y	20.2	8.3	8.6
Y123F	16.0	11.0	3.6
Y165F	14.0	7.8	7.6
Y191F	12.5	9.0	3.5
Y191H	40.0	9.5	6.3
Y123F/Y165F	−	−	0
Y123F/Y191F	80	22	<0.1
R164L	19.0	9.0	6.3
R164L/Y165L	55	ND[b]	0.7
H231A	40	ND[b]	10
D383A	33	ND[b]	11.5
H230A	9.5	ND[b]	6.7

[a] All mutants had identical properties. [b] Not determined.

The double mutant Y123F/Y191F has an 8-fold increased K_m for iron, a 2-fold increased K_m for porphyrin, and low activity. The conserved residue W227 was mutated to W227Y and found to have a 2-fold increase in K_m for iron, but little change in V_{max} or K_m for porphyrin.

Characteristics of Arginyl and Histidyl Residues. R164 was mutated since it is located in the active site pocket adjacent to Y165 opposite from H263. The R164L mutant has a normal K_m for porphyrin, but a 2-fold increased K_m for iron. The double mutant R164L/Y165F exhibits a 6-fold increased K_m for iron and a 10-fold decrease in V_{max}.

The H263A, H263N, and H263C mutants were produced, and all of these enzymes as isolated possess intact and stable [2Fe-2S] clusters; however, in contrast to published claims for H263A (*36*), none of these proteins have any enzyme activity, and none complement the ferrochelatase deficient *E. coli* Δ*hemH*. All of these mutants have bound protoporphyrin as isolated (413 nm), and this is not converted into protoheme upon storage (Figure 2). Incubation of H263A with 300 mM imidazole overnight did not result in the conversion of porphyrin to heme, suggesting that the exogenously supplied imidazole could not intercalate into the complex structure and replace the missing side chain of H263. The H341C mutant was found to have kinetic parameters similar to those of some of the carboxylate residue mutants described above. It has essentially unchanged K_ms for both substrates but a decreased V_{max}. The H341C protein as isolated contains no residual porphyrin or protoheme (Figure 2).

Characteristics of D383, H230, and H231. From the crystal structure of human ferrochelatase, it was shown that exogenously added Co^{2+} was bound to the protein via ligation by D383 and H231 (*31*). These two residues were individually mutated to alanine, and the adjacent H230 was changed to an alanine. Kinetic data (Table 2) show that the D383A and H231A mutants both had a decreased affinity for iron as would be anticipated if these residues were

```
human          MRSLGANMAAALRAAGVLLRDPLASSSWRVCQPWRWKSGAAAAAVTTCTAQHAQGAKPQVQPQKRKPKTGILMLN
s_cerevesiae   ~~~~~~~~~~~~~~~~~~~~~~~~~~~~MLSRTIRTQGSFLRRSQLTITRSFSVTFNMQ.NAQKRSP.TGIVLMN
b_subtilis     ~~~~~~~~~~~~~~~~~~~~~~~~~~~~~~~~~~~~~~~~~~~~~~~~~~~~~~~~~~~~~~~MSRKKMGLLVMA
               1........10........20........30........40........50........60........70....

human          MGGPETLGDVHDFLLRLFLDRDLMTL..PIQNKLAPFIAKRRTPKIQEQYRRIGGGSPIKIWTSKQGEGMVKLLD
s_cerevesiae   MGGPSKVEETYDFLYQLFADNDLIPISAKYQKTIAKYIAKFRTPKIEKQYREIGGGSPIRKWSEYQATEVCKILD
b_subtilis     YGTPYKEEDIERYYTHIRRGRK..PEPEMLQD.............LKDRYEAIGGISPLAQITEQQAHNLEQHLN
               ....80........90........100.......110.......120.......130.......140........

human          ELSPNTAPHKYYIGFRYVHPLTEEAIEEMERDGLERAIAFTQYPQYSCSTTGSSLNAIYRYYNQVGRKPTMKWST
s_cerevesiae   KTCPETAPHKPYVAFRYAKPLTAETYKQMLKDGVKKAVAFSQYPHFSYSTTGSSINELWRQIKALDSERSISWSV
b_subtilis     EIQDEIT.FKAYIGLKHIEPFIEDAVAEMHKDGITEAVSIVLAPHFSTFSV.QSYNK..RAKEEAEKLGGLTITS
               151......160.......170.......180.......190.......200.......210.......220...

human          IDRWPTHHLLIQCFADHILKELDHFPLEKRSEVVILFSAHSLPMSVVNRGDPYPQEVSATVQKVMERLEYCNPYR
s_cerevesiae   IDRWPTNEGLIKAFSENITKKLQEFPQPVRDKVVLLFSAHSLPMDVVNTGDAYPAEVAATVYNIMQKLKFKNPYR
b_subtilis     VESWYDEPKFVTYWVDRVKETYASMPEDERENAMLIVSAHSLPEKIKEFGDPYPDQLHESAKLIAEGAGV.SEYA
               ....230.......240.......250.......260.......270.......280.......290........

human          LVWQSKVG.PMPWLGPQTDESIKGLCE.RGRKNILLVPIAFTSDHIETLYELDIEYSQVLAKECGVENIRRAESL
s_cerevesiae   LVWQSQVG.PKPWLGAQTAEIAEFLGP.K.VDGLMFIPIAFTSDHIETLHEIDL...GVIGESEYKDKFKRCESL
b_subtilis     VGWQSEGNTPDPWLGPDVQDLTRDLFEQKGYQAFVYVPVGFVADHLEVLYDNDYE.CKVVTDDIGA.SYYRPEMP
               301......310.......320.......330.......340.......350.......360.......370...

human          NGNPLFSKALADLVHSHIQSNELCSKQLTLSCPL.CVNPVCRETKSFFTSQQL~
s_cerevesiae   NGNQTFIEGMADLVKSHLQSNQLYSNQLPLDFALGKSNDPVKDLSLVFGNHEST
b_subtilis     NAKPEFIDALATVVLKKLGR~~~~~~~~~~~~~~~~~~~~~~~~~~~~~~~~~~
               ....380.......390.......400.......410.......420.......
```

FIGURE 1: Pile-up analysis of selected ferrochelatases. Sequences shown are for the human, *Saccharomyces cerevisiae*, and *B. subtilis* enzymes. Identical residues among sequences in this alignment are shown in black boxes. The numbering is for the Pile-up alignment and does not correspond strictly to any of the individual sequences shown due to the insertion of spaces to optimize the alignment.

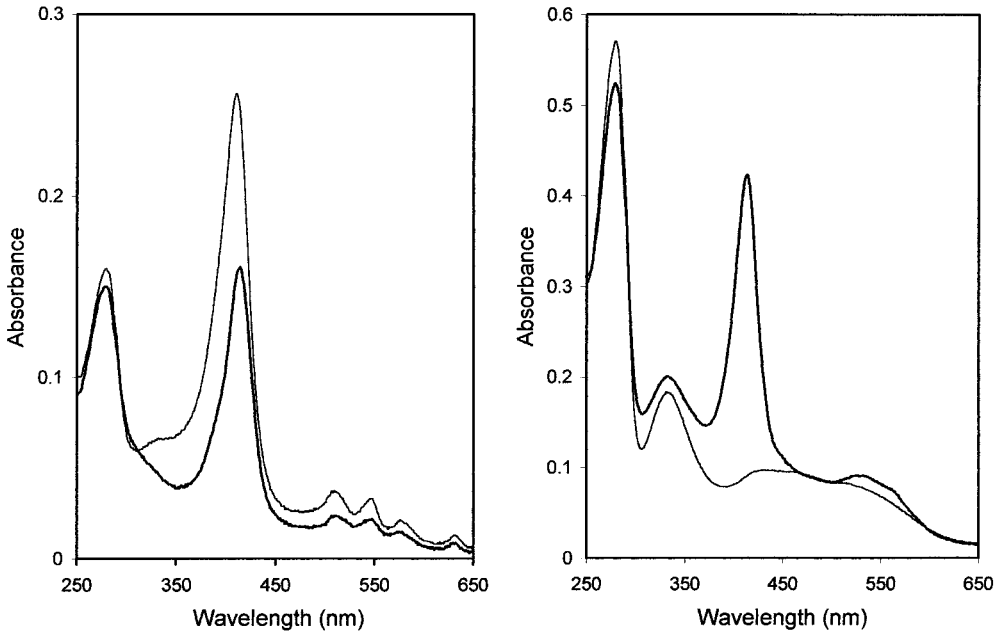

FIGURE 2: UV−visible spectra of human ferrochelatase mutants. In the spectra shown on the left, the highest absorbance (at 410 nm) is for the mutant E343K (3.2 μM) while the spectrum for E343H (3.0 μM) has a lower Soret absorbance with a maximum at 413 nm. Due to the large porphyrin absorbance, the typical [2Fe-2S] cluster features at 320 and 450−550 nm are not distinguishable. The spectra shown on the right are for human ferrochelatase H263C (11.6 μM) and H341C (10.4 μM) mutants. The spectrum for the H263C mutant enzyme exhibits a distinctive Soret absorbance at 412 nm, while the H341C mutant has no apparent Soret and exhibits only features of the [2Fe-2S] cluster.

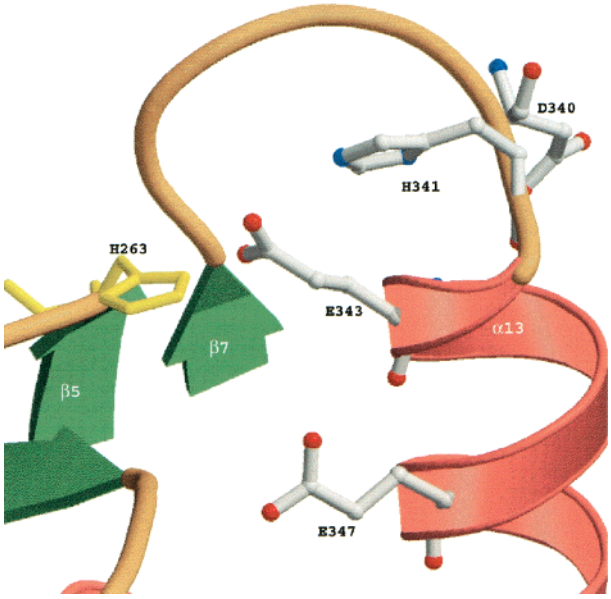

FIGURE 3: Cross section of the lower lip of human ferrochelatase showing the spatial relationship of H263 to the adjacent conserved residues D340, H341, E343, and E347. All of these residues reside on the same side of the pocket with the distance between H263 and E343 being approximately 3 Å. The numbering of structural features in the diagram is that of Wu et al. (*31*).

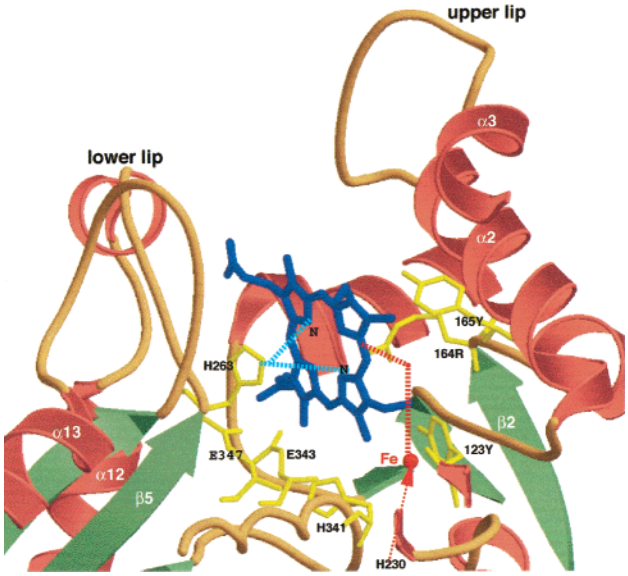

FIGURE 4: Cross section through the active site pocket of human ferrochelatase showing the location of key residues and the proposed catalytic model for human ferrochelatase. The porphyrin substrate enters into the active site pocket from the membrane (top of the figure), and iron is shown to enter (dashed red line) from the previously identified site at H231/D383 (*31*). Residues H263, E343, H341, and D340 are proposed to be involved in the two-proton extraction from the pyrrole NHs (dashed blue lines). Porphyrin metalation occurs from R164 and Y165 which are on the opposite side of the pocket from H263.

involved in substrate−iron binding. Interestingly, H230A exhibited little alteration in enzyme activity from wild-type parameters even though in human ferrochelatase H231 is located adjacent to H230 in the structure (*31*).

DISCUSSION

The enzymatic reaction catalyzed by ferrochelatase, the insertion of a divalent cation into a planar macrocycle, is interesting from both a chemical and thermodynamic viewpoint. During catalysis, the enzyme transiently binds ferrous iron, protoporphyrin, and heme. For metalation to occur, several criteria must be met: (1) porphyrin ring distortion, (2) outer-sphere complexation, (3) dissociation of the iron−ligand complex, and (4) pyrrole proton loss (*25*). To satisfy these demands, ligands must exist which will bind the substrates with sufficient avidity and specificity to facilitate catalysis, but must be arranged so that subsequent product release is favorable. Solution studies of porphyrin metalation

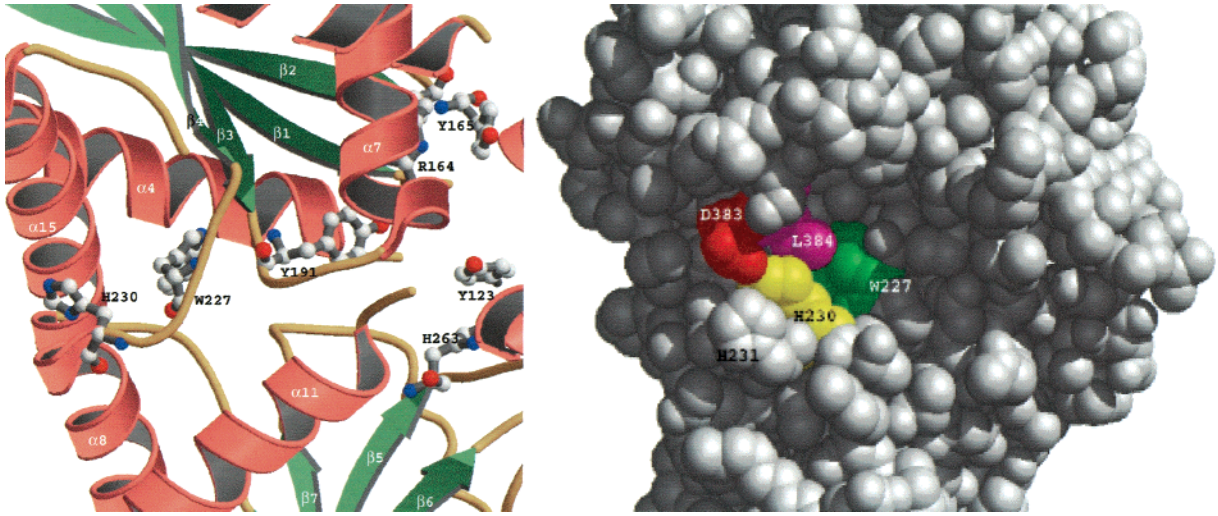

FIGURE 5: Position of putative iron-binding residues in human ferrochelatase. On the left is a cross-section ribbon diagram of human ferrochelatase showing the positions of putative iron-binding and metalation residues. The diagram illustrates the position of residues D383 and H231 which have been demonstrated to bind exogenously supplied cobalt (*31*), and residues W227, Y191, R164, and Y165 which are suggested to be involved Fe^{2+} transport into the active site. Y123 is also shown along with the position of H263. Residues H231, W227, Y191, R164, and Y165 are linearly aligned with Y191 being at the bottom of the active site pocket. R164 and Y165 are located in the center of the pocket and are directly opposite from H263. In this view, Y123 is located well behind these other residues. On the right is shown a space-filling diagram with the locations of D383, H231, and W227 given. L384 and H231 are labeled, but are not highly conserved residues among all ferrochelatases.

reactions show that ferrous iron is inserted into protoporphyrin and displaces the two pyrrole protons, rather than having porphyrin deprotonation occurring prior to metal insertion (*37*, *38*). Thus, it is likely that the exit route taken by the two pyrrole protons is on the opposite side of the macrocycle from which the iron initially approaches. In the current study, we have examined residues that may be involved in proton abstraction and substrate−iron ligation.

Previously, H263 had been suggested to be a substrate iron ligand based upon a reported alteration in the K_m for iron in an H263A mutant (*36*). However, it is clear from the current study that ferrochelatase with H263 replaced with Ala, Asn, Met, or Cys has no enzyme activity and that the kinetic data reported by Kohno et al. (*36*) must have been able to be attributed to contaminating *E. coli* ferrochelatase that was present in the crude cell extracts used by these workers. The fact that all mutants at H263 have no measurable activity does not eliminate this residue as a potential iron ligand, but strongly suggests that its role must be key to catalysis. Mutation of this corresponding histidyl residue in ferrochelatases of *Drosophila melanogaster* and *E. coli* also resulted in a total loss of activity (data not shown). On the basis of these data and the spatial position of H263 in the active site, we suggest that H263 is not an iron ligand, but plays the key role as an acceptor of a proton from the porphyrin macrocycle. Such a role is common for active site histidyl residues in a variety of other enzymes.

It has been suggested that the highly conserved carboxylate residues D340, E314, and E347 may be involved in porphyrin proton abstraction (*1*, *39*). If these residues participate in proton abstraction from the porphyrin ring during catalysis, then substitution of these carboxylates with the corresponding amides or conversion into a basic residue would be expected to slow or block the removal of protons, leading to an enzyme with substrate(s) bound, but little or no product formation. The results of the experiments described above for purified human ferrochelatase demonstrate that the mutants E343Q/H/K and D340N all have no measurable enzyme activity and contain bound protoporphyrin, not protoheme, when they are isolated. Ferrochelatases that possess mutations in this region that are less severe (i.e., D340E, E343D, and E347Q) still possess enzyme activity and have unaltered K_ms for both substrates, but decreased V_{max}s. Located near the conserved carboxylates is H341 (Figure 3) which, when mutated to H341C, behaved in a fashion similar to that of the carboxylate residue mutants, suggesting that it may also play a role in proton abstraction. These data imply that alteration of the carboxyl rich region effects enzyme turnover, but does so without altering the affinity of the enzyme for either of its substrates. Thus, the role of the carboxyl rich region, which is located immediately adjacent to H263 (Figure 3), may be to serve as a conduit for the pyrrole protons to be shuttled out of the active site. This conclusion is consistent with data from studies with cytochrome oxidase (*40*) and bacteriorhodopsin (*41*) which provide characterized models for side chain carboxylates in proton movement. Support for the pyrrole proton shuttle model may come from higher-resolution crystallographic data of wild-type and mutant human ferrochelatases that should reveal hydrogen-bonding patterns among these residues.

It has been suggested that in the *B. subtilis* ferrochelatase (*27*, *30*) and the cobalt chelatase of *Salmonella typhimurium* (*42*) the residues corresponding to human H263, D340, E343, and E347 may play a role in substrate metal binding as well as proton abstraction. However, it seems unlikely from steric considerations and solution porphyrin metalation studies (*37*, *38*) that these residues participate in both proton abstraction and substrate−iron binding. While it may be that H263 helps to "pull" the iron into the macrocycle and, thereby, facilitates metalation, the localization of H263 on the same side of the pocket as D340, E343, H341, and E347 would mean that the residues responsible for initially coordinating the substrate iron must reside on the opposite side of the catalytic pocket.

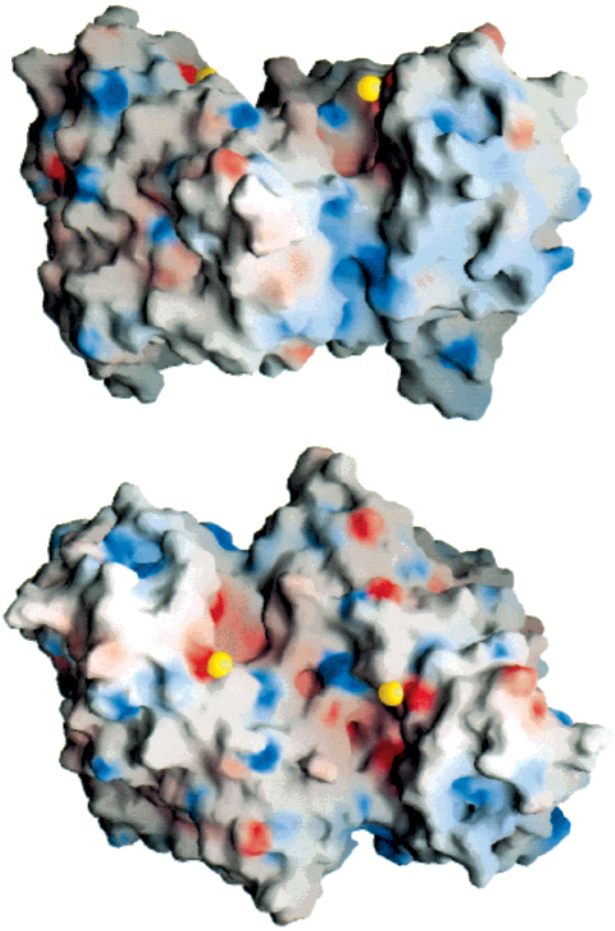

FIGURE 6: Surface potential diagram of human ferrochelatase with bound cobalt. Acidic residues are red and basic regions are blue. The cobalt atom is shown as a yellow ball. The dimer is shown with the dimer interface occurring in the middle of the figure. The bottom figure represents the top of the molecule if one considers the active site pocket-containing surface which is proposed to be located in the membrane to represent the bottom of the molecule. Because this surface of the protein is directly opposite from the active site entrance and the 2-fold symmetry of the dimer, both putative iron-binding sites are located on a common surface and would be exposed to the mitochondrial matrix. The top view represents a side view of the dimer. The site of one bound metal is clearly visible at the back of a recessed pocket.

X-ray crystallographic studies of a *B. subtilis* ferrochelatase−*N*-methylmesoporphyrin complex crystal with exogenously supplied copper clearly demonstrated demethylation of the alkylated porphyrin, and insertion of copper into the distorted macrocycle (*27*). From these data, the authors suggested that metalation with iron may occur from the histidyl side of the pocket and involve the equivalent of human H263 and E343. Two pieces of data that are significant in this study is that neither demethylation nor metal binding was observed with Zn^{2+} and that a metalation pathway involving only this portion of the active site cannot account for the difference in metal specificity seen with the *B. subtilis* ferrochelatase versus other characterized ferrochelatases. Since the kinetic data presented above for the mutants of the carboxylate rich region are not consistent with a role for these residues in iron binding, we would suggest that the copper cation adventiously binds to the anionic carboxylate patch of the *B. subtilis* enzyme−porphyrin complex and migrates to the available histidyl residue where it then reacts with the alkylated porphyrin, catalyzing the demethylation.

On the basis of studies of inhibition of ferrochelatase by a Zn−*N*-methylporphyrin species, Lavallee (*25*) has proposed that one of the ferrous iron ligands of ferrochelatase may include a Lewis base, and R164 of human (K87 of *B. subtilis*) may serve that role. The side chains of R164 and Y165 are centrally located in the active site pocket directly opposite H263 in a position that would appear to be ideal for final iron binding prior to porphyrin metalation (Figure 4). A role for these residue side chains in metalation is also strongly supported by the kinetic parameters of the R164L and Y165F mutants. While it seems a bit unusual that the ligands for ferrous iron in ferrochelatase would include tyrosyl residues rather than carboxylates, the presence of acidic side chains in the proximity of the metalation site may favor the reverse reaction, demetalation (*38*). Tyrosyl residues, especially in tandem, are common ligands for stable ferric iron chelates; however, in ferrochelatase, there is a need for only a transient ferrous iron−ligand interaction, and it is clear from the structure that at no time could the iron molecule be simultaneously ligated by two tyrosyl side chains. Y123, which is also highly conserved and on the same "lip" as R164 and Y165, is spatially too distant to simultaneously participate in the coordination of iron unless there is significant molecular movement.

H231 and D383 were identified in the crystal structure of human ferrochelatase as ligands for exogenously supplied cobalt, thereby suggesting that this site may represent the initial binding site for substrate iron (*31*) (see Figure 5). However, this site is located on the opposite side of the molecule from the active site opening and is more than 20 Å from H263 at the center of the active site. Thus, additional residues must be involved in the movement of iron into the active site and in porphyrin metalation. Interestingly, there are a number of conserved residues (W227, Y191, R164, and Y165) that appear to span the region from H231/D383 to the active site (Figure 5). Ferrochelatases with mutations at W227, Y191, R164, and Y165 have altered substrate metal affinities without an alteration in porphyrin affinity (Table 2) as one would expect for residues involved in metal coordination. Both W227 and Y191 are too distant from the active site to serve a role in direct metalation, but may serve a role in the movement of the iron from H231 to R164/Y165. It is of note that ferrochelatase of *B. subtilis*, which does not use Co^{2+} like human ferrochelatase, but instead will use Cu^{2+}, has only W227 conserved and, as in other Gram-positive bacterial ferrochelatases, does not possess R164, Y165, and Y191. Instead, it has K87 (164), H88 (165), and A114 (191).

On the basis of the data presented above and previously, we propose a model where iron binds initially at H231 and D383 in human ferrochelatase and is translocated by a group of highly conserved residues (W227 and Y191) into the interior of the protein at the enzyme's active site. Actual metalation into the distorted porphyrin macrocycle would occur from R164 and Y165 with simultaneous proton abstraction mediated by H263 and the conserved carboxylates (Figure 4). This model implies that in human ferrochelatase access to the active site occurs via two distinct routes for the two substrates. Porphyrin enters the active site from the membrane-facing surface, while iron approaches from the

surface of the molecule that is exposed to the mitochondrial matrix. Interestingly, the identified metal binding site at D383 is located within a pocket-like feature which could be envisioned as a potential docking site for an iron donor or transporter protein (Figure 6). This proposal is consistent with a previous suggestion that iron for heme synthesis in yeast is linked to a specific mitochondrial transport system (*43*, *44*). It should be noted that this model may be general only for mitochondrial-associated eukaryotic ferrochelatases since the spatial orientation of ferrochelatase within prokaryotic cells may differ, especially for the soluble ferrochelatases such as that found in *B. subtilis*. In these instances, iron entry may occur via a slightly different route, but would still be expected to result in metalation in the active site from the opposite side of the porphyrin macrocycle as deprotonation occurs.

ACKNOWLEDGMENT

We acknowledge A. E. Burden for preparation of some of the mutant proteins used in this study.

REFERENCES

1. Dailey, H. A. (1996) in *Mechanisms of Metallocenter Assembly* (Hausinger, R. P., Eichhorn, G. L., and Marzilli, L. G., Eds.) pp 77−98, VCH Publishers, New York.
2. Porra, R. J., Vitols, K. S., Labbe, R. F., and Newton, N. A. (1967) *Biochem. J. 104*, 321−327.
3. Karr, S. R., and Dailey, H. A. (1988) *Biochem. J. 254*, 799−803.
4. Harbin, B. M., and Dailey, H. A. (1985) *Biochemistry 24*, 366−370.
5. Jones, M. S., and Jones, O. T. G. (1969) *Biochem. J. 113*, 507−514.
6. Miyamoto, K., Nakahashi, K., Nishimura, K., and Inokuchi, H. (1991) *J. Mol. Biol. 219*, 393−398.
7. Frustaci, J. M., and O'Brian, M. R. (1993) *J. Bacteriol. 175*, 2154−2156.
8. Frustaci, J. M., and O'Brian, M. R. (1992) *J. Bacteriol. 174*, 4223−4229.
9. Hansson, M., and Hederstedt, L. (1992) *J. Bacteriol. 174*, 8081−8093.
10. Labbe-Bios, R. (1990) *J. Biol. Chem. 265*, 7278−7283.
11. Smith, A. G., Santana, M. A., Wallace-Cook, A., Roper, J. M., and Labbe-Bois, R. (1994) *J. Biol. Chem. 269*, 13405−13413.
12. Nakahashi, Y., Taketani, S., Okuda, M., Inoue, K., and Tokunaga, R. (1990) *Biochem. Biophys. Res. Commun. 173*, 748−755.
13. Taketani, S., Nakahashi, Y., Osumi, T., and Tokunaga, R. (1990) *J. Biol. Chem. 265*, 19377−19380.
14. Brenner, D. A., and Frasier, F. (1991) *Proc. Natl. Acad. Sci. U.S.A. 88*, 349−353.
15. Day, A. L., Parsons, B. M., and Dailey, H. A. (1998) *Arch. Biochem. Biophys. 359*, 160−169.
16. Dailey, H. A., Finnegan, M. G., and Johnson, M. K. (1994) *Biochemistry 33*, 403−407.
17. Dailey, H. A., Sellers, V. M., and Dailey, T. A. (1994) *J. Biol. Chem. 269*, 390−395.
18. Ferreira, G. C., Franco, R., Lloyd, G. S., Pereira, A. S., Moura, I., Moura, J. J. G., and Huynh, B. H. (1994) *J. Biol. Chem. 269*, 7062−7065.
19. Crouse, B. R., Sellers, V. M., Finnegan, M. G., Dailey, H. A., and Johnson, M. K. (1996) *Biochemistry 35*, 16222−16228.
20. Sellers, V. M., Johnson, M. K., and Dailey, H. A. (1996) *Biochemistry 35*, 2699−2704.
21. Sellers, V. M., Wang, K.-F., Johnson, M. K., and Dailey, H. A. (1998) *J. Biol. Chem. 273*, 22311−22316.
22. Hansson, M., and Hederstedt, L. (1994) *Eur. J. Biochem. 220*, 201−208.
23. Dailey, H. A. (1987) *Ann. N.Y. Acad. Sci. 514*, 81−86.
24. Dailey, H. A., and Fleming, J. E. (1983) *J. Biol. Chem. 258*, 11453−11459.
25. Lavallee, D. K. (1988) in *Mechanistic Principles of Enzyme Activity* (Liebman, J. F., and Greenberg, A., Eds.) pp 279−314, VCH Publishers, New York.
26. Blackwood, M. E., Rush, T. S., Medlock, A., Dailey, H. A., and Spiro, T. G. (1997) *J. Am. Chem. Soc. 119*, 12170−12174.
27. Lecerof, D., Fodje, M., Hansson, A., Hansson, M., and Al-Karadaghi, S. (2000) *J. Mol. Biol. 297*, 221−232.
28. Blackwood, M. E., Rush, T. S., Romesberg, F., Schultz, P. G., and Spiro, T. G. (1998) *Biochemistry 37*, 779−782.
29. Franco, R., Ma, J.-G., Lu, Y., Ferreira, G. C., and Shelnutt, J. A. (2000) *Biochemistry 39*, 2517−2529.
30. Al-Karadaghi, S., Hansson, M., Nikonov, S., Jönsson, B., and Hederstedt, L. (1997) *Structure 5*, 1501−1510.
31. Wu, C.-K., Dailey, H. A., Rose, J. P., Burden, A. M., Sellers, V. M., and Wang, B.-C. (2001) *Nat. Struct. Biol. 8*, 156−160.
32. Burden, A. E., Wu, C.-K., Dailey, T. A., Busch, J. L. H., Dhawan, I. K., Rose, J. P., and Wang, B.-C. (1999) *Biochim. Biophys. Acta 1435*, 191−197.
33. Deng, W. P., and Nickoloff, J. A. (1992) *Anal. Biochem. 200*, 81−88.
34. Furhop, J.-H., and Smith, K. M. (1975) in *Porphyrins and Metalloporphyrins* (Smith, K. M., Ed.) pp 757−869, Elsevier, Amsterdam.
35. Rufenacht, U. B., Gouya, L., Schneider-Yin, X., Puy, H., Schafer, B. W., Aquaron, R., Nordmann, Y., Minder, E. I., and Deybach, J. C. (1998) *Am. J. Hum. Genet. 62*, 1341−1352.
36. Kohno, K., Masahiro, O., Furukawa, T., Tokunaga, R., and Taketani, S. (1994) *Biochim. Biophys. Acta 1209*, 95−100.
37. Bain-Ackerman, M. J., and Lavallee, D. K. (1979) *Inorg. Chem. 18*, 3358−3364.
38. Hambright, P. (1975) in *Porphyrins and Metalloporphyrins* (Smith, K., Ed.) pp 233−278, Elsevier, Amsterdam.
39. Gora, M., Grzybowska, E., Rytka, J., and Labbe-Bois, R. (1996) *J. Biol. Chem. 271*, 11810−11816.
40. Adelroth, P., Ek, M. S., Mitchell, D. M., Gennis, R. B., and Brzezinski, P. (1997) *Biochemistry 36*, 13824−13829.
41. Luecke, H., Schobert, B., Richter, H.-T., Cartailler, J.-P., and Lanyi, J. K. (1999) *Science 286*, 255−260.
42. Schubert, H. L., Raux, E., Wilson, K. S., and Warren, M. J. (1999) *Biochemistry 38*, 10660−10669.
43. Lange, H. G., and Kispal, R. L. (1999) *J. Biol. Chem. 274*, 18989−18996.
44. Lange, H. G., and Kispal, R. L. (1999) *J. Biol. Chem. 286*, 255−260.

BI010012C